Particle-in-cell simulation of collisionless reconnection with open outflow boundaries

Alex Klimas,[1] Michael Hesse,[2] and Seiji Zenitani[3]
[1]*UMBC at NASA Goddard Space Flight Center, Greenbelt, Maryland 20771, USA*
[2]*NASA Goddard Space Flight Center, Greenbelt, Maryland 20771, USA*
[3]*ORAU at NASA Goddard Space Flight Center, Greenbelt, Maryland 20771, USA*

(Received 19 May 2008; accepted 10 July 2008; published online 4 August 2008)

A new method for applying open boundary conditions in particle-in-cell (PIC) simulations is utilized to study magnetic reconnection. Particle distributions are assumed to have zero normal derivatives at the boundaries. Advantages and possible limitations of this method for PIC simulations are discussed. Results from a reconnection simulation study are presented. For the purpose of this investigation, a $2\frac{1}{2}$-dimensional electromagnetic PIC simulation using open conditions at the outflow boundaries and simple reflecting boundaries to the inflow regions is discussed. The electron diffusion region is defined as that region where the out-of-plane electron inertial electric field is positive indicating acceleration and flux transfer; the evolution of this region is analyzed. It is found that this region varies in the range 2.5–4 local electron inertial lengths in total width and in the range 10–15 local electron inertial lengths in total length for the mass ratio 25. The reconnection rate is investigated in terms of the aspect ratio of the electron diffusion region plus inflow and outflow measures at its boundaries. It is shown that a properly measured aspect ratio predicts the flux transfer rate, scaled to account for the decline in field strength and electron density at the inflow boundary to the electron diffusion region. It is concluded that this electron diffusion region either adjusts its aspect ratio for compatibility with the flux transfer rate that is set elsewhere, as in the Hall reconnection model, or that it is this region that controls the reconnection flux transfer rate.
 [DOI: 10.1063/1.2965826]

I. INTRODUCTION

Collisionless magnetic reconnection is a central process in many plasma systems of interest. It is thought to play an important role in the solar corona,[1–5] in the solar wind,[6–8] in the interaction of the solar wind with Earth's and other planetary magnetospheres,[9–12] in the interiors of these magnetospheres,[13–16] in laboratory plasma devices,[17–19] and in astrophysical settings.[20,21] To understand the evolution of these systems, it is necessary to understand the reconnection process and its contribution to the system dynamics.

Much of what is known about collisionless reconnection has been learned from numerical plasma-simulation experiments. A central issue in these studies is the nature of the dissipation mechanism that replaces the resistivity of collision dominated reconnection. A "Hall reconnection model"[22–30] has emerged in which there exists a small region of electron diffusion, with thickness on the order of the electron inertial length, in which the magnetic flux transfer from one topological region to another occurs. This electron diffusion region is embedded within a larger ion diffusion region, with thickness on the order of the ion inertial length. The overall reconnection rate is governed by the larger scale evolution of the ions, with the electron diffusion region adjusting to accommodate this rate, and with electron thermal and bulk inertial effects providing the reconnection electric field of the electron diffusion region. In this model, the lengths of both the ion and electron diffusion regions remain sufficiently small to permit fast reconnection.

Daughton *et al.*,[31] however, have challenged the Hall reconnection model based on the results of their study using a $2-1/2$-dimensional electromagnetic particle-in-cell (PIC) reconnection simulation model with open boundaries. As a direct consequence of the open boundaries, they were able to extend their simulations to longer times than are feasible in simulations using periodic boundary conditions. Daughton *et al.* compared their open boundary simulation results to the results of a simulation using periodic boundaries on a large simulation grid. They found general agreement between their two types of simulations for earlier times but found that for later times the two types diverged and the evolution of the open boundary simulation was in disagreement with the Hall reconnection model. As the open boundary simulations advanced in time, the reconnection rate gradually slowed to a value much lower than indicated by the Hall model. They argued that the electron diffusion region in their open boundary simulations gradually lengthened in the directions of the outgoing jets, and, as it lengthened, the reconnection rate slowed accordingly. Although this lengthening was occasionally interrupted by the formation of magnetic islands leading to the division of the extended region into parts and to large fluctuations in the reconnection rate, the overall trend was to a diffusion region of the order of tens of ion inertial lengths in the outflow directions but of the order of the electron inertial length in thickness. It is important to note that they demonstrated this phenomenon in two measures of the diffusion region; the length of the out-of-plane electron current sheet supporting the field reversal plus the coincident length of the region in which the magnetohydrodynamic (MHD)

approximation to the electric field, $\mathbf{E}=-\mathbf{V}\times\mathbf{B}$, was violated. In a later paper, Karimabadi *et al.*[32] supported and expanded these results. They showed that there is an outer region of the diffusion region, as they defined it, where the electron outflow jets move faster than the $\mathbf{E}\times\mathbf{B}$ drift. In the diffusion region proper, electrons are accelerated in the out-of-plane direction and turned toward the outflow direction by the Lorentz force. In the outer region, the outflow jet gradually slows down and dissipates. They showed that the dynamics of these two regions can be in equilibrium for extended intervals in time during which the reconnection rate is relatively constant and, for the two examples given, fast. At other times in their simulations, magnetic island formation leads to large fluctuations in the reconnection rate. Overall, Daughton *et al.* and Karimabadi *et al.* conclude that the Hall reconnection picture with the reconnection rate defined by the larger scale ion evolution and with the electron diffusion region measured in the outflow directions in electron inertial lengths is a picture drawn from the limited results of simulations using periodic boundary conditions, which are not valid over the large time scales relevant to physical systems.

Fujimoto[33] has shown related behavior in the electron diffusion region using $2-1/2$-dimensional electromagnetic PIC simulations with periodic boundary conditions. An adaptive mesh refinement technique as well as particle splitting was used to enable large-scale full particle simulations. A sequence of simulations was carried out in which the length of the simulated region was increased until the results were independent of the length, thus demonstrating the irrelevance to the results of the periodic boundary conditions. In this study, the electron diffusion region was defined as that region where the out-of-plane velocity of the electrons is high, bounded in the outflow directions by the positions of the maxima in the electron outflow velocities. Fujimoto showed a peaking and then decreasing reconnection rate with the onset of the decrease coincident with the establishment of a polarization electric field in the inflow directions from above and below in the vicinity of the X-line. This polarization field was supported by charge separation between a broader distribution of primarily meandering cold background ions and a very narrow electron distribution, established at this time in the simulation. The polarization field led to a localized region of strong out-of-plane electron drift that expanded in the outflow directions leading to an extending electron diffusion region and to a consequent decline in the reconnection rate.

Shay *et al.*[34] have carried out a series of PIC reconnection simulations with varying electron to ion mass ratio and simulation domain size. Although these were periodic simulations, Shay *et al.* showed that the boundaries could not affect the reconnection process over the course of the simulations because of the sizes of the simulation domains that they used. Indeed, they found a universal steady fast reconnection rate for a variety of mass ratios and system sizes with no evidence of magnetic island formation after some initial transients in the simulations. While their simulations showed no evidence of slowing reconnection rate with increasing time, they also found themselves in some agreement with the results of Daughton *et al.*[31] and in particular Karimabadi *et al.*[32] with respect to the properties of the electron outflow region. They showed an extended electron diffusion region with inner and outer parts as discussed by Karimabadi *et al.* but with an electron out-of-plane current sheet whose length stabilizes in time at a value that decreases with increasing ion to electron mass ratio.

At present, it is clear that a significant degree of uncertainty exists concerning the correct description of collisionless reconnection. An important contribution could be made through an independent simulation study using open boundary conditions. Toward that end, in this paper we introduce a new method for applying open boundary conditions to PIC simulations and we present first reconnection simulation results using this method. To open the boundaries, Daughton *et al.*[31] enforced zero normal derivatives at the boundaries on the moments of the particle distributions, from the density up to the pressure tensor, for each of the particle species. We extend this idea to apply zero normal derivatives at the boundaries to the particle distributions themselves.

We discuss the results of a $2\frac{1}{2}$-dimensional PIC simulation using open conditions at the outflow boundaries and simple reflecting boundaries to the inflow regions. Our method for imposing open boundary conditions is described in Sec. II. Following that section, the simulation setup is discussed in Sec. III and then our simulation results are presented in Sec. IV. Further, we compare the results of the open boundary simulation to those of a periodic simulation on an extended domain to verify the validity of our open boundary construct. This discussion appears in the Appendix. In contrast to the papers discussed above, we define the electron diffusion region as that region where the topological magnetic flux transfer takes place, based on the sign of the electron inertial contribution to the out-of-plane electric field. Our principal finding is that it is this region that controls the reconnection rate.

II. OPEN BOUNDARY CONSTRUCT

Conceptually, our new open boundary algorithm is quite simple. Consider the open boundary at $x=x_{\min}=0$ illustrated in Fig. 1. All particle-containing cells just inside this boundary are contained in column 1, the next column of cells is labeled column 2, and so on. For every particle in column 1, we assume that there is an identical particle at the same velocity and relative position in a column of ghost cells just outside of the boundary; it is not necessary to actually incorporate the ghost cells into the simulation code. In this manner, we impose a zero normal gradient on the particle distributions at the boundary. As usual, the position and velocity of each particle is stored. Any particle that moves from within column 1 through the boundary at $x=0$ is discarded. In addition, the initial and final positions of each particle are checked at each integration step in time. If a particle moves from column 1 to column 2, then it is assumed that there was an identical particle in the column of ghost cells that has moved into column 1. In this case, a new particle is introduced at the appropriate position and velocity in column 1 and it is carried forward in time from that point on. Thus, the passage of particles through the boundary to maintain a zero

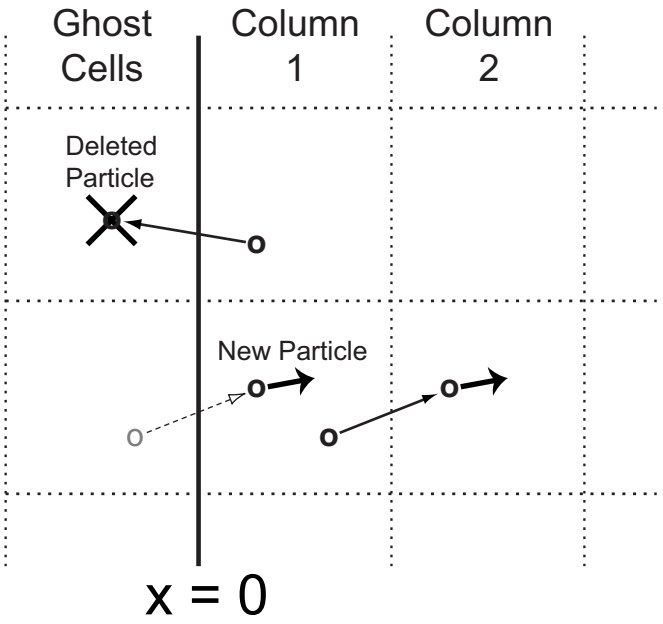

FIG. 1. Open boundary construct for zero-gradient particle distribution at boundary: For every particle in column 1 there is an identical ghost particle at the same velocity and relative position in a column of ghost cells just outside of the boundary. If a particle moves from column 1 to column 2, then a ghost particle moves into column 1 and becomes a new particle at the appropriate position and velocity. Any particle that moves from column 1 through the boundary at $x=0$ is deleted.

normal gradient for the particle distributions has been achieved. The biggest difficulty with this construct is keeping track of particles lost and gained, but this can be done easily with very little additional computational load.

For the simulation discussed here, we have used the 2 $\frac{1}{2}$-dimensional electromagnetic PIC code described in Hesse *et al.*,[23] modified to incorporate this open boundary construct on the outflow boundaries of the simulation domain. Densities and fluxes are accumulated on a grid using a rectangular particle shape function. Ghost particles contribute to the densities and fluxes at the open boundaries at each time step. Charge conservation is guaranteed by an iterative application of a Langdon–Marder type[35] correction to the electric field at each time step. A gradient-free electric field is used as an initial choice at the open boundaries (the field is extrapolated with zero gradient), following which the Langdon–Marder iterative algorithm corrects the electric field over the entire simulation grid, including the boundaries. The electromagnetic fields are integrated implicitly to avoid the Courant constraint on the propagation of light waves.[23] Using the implicit solver for the electromagnetic field, we impose the following conditions: zero normal gradient for the tangential magnetic field and div B=0 for the normal component on the open boundaries. These choices lead to smooth passage of electromagnetic structures (magnetic islands, outflow jets, etc.) through the boundaries with no trace of charge buildup near the boundaries or anywhere else on the computational grid. No smoothing is applied to either the particle distributions or the fields at the boundaries.

Because this open boundary construct deals directly with particles rather than their moments, it has several advantages for PIC simulations; it is simple to program, it is computationally fast, it is more general than the moment approach, and we have found that in practice it requires no smoothing whatsoever. It must be recognized, however, that there may be limitations to such an approach. As explained above, particles are injected into the first column of cells inside an open boundary at exactly the velocity and relative position of particles that have moved from the first to the second column of cells inside the boundary. Thus, unphysical particle correlations may be introduced at the open boundaries. It is not clear if such correlations can have physical consequences in the simulation. For the simulation discussed below, we have found no evidence of any disturbance propagating into the interior of the simulation domain due to these correlations. However, this issue will require careful monitoring as we proceed further with this open boundary technique in the future.

III. SIMULATION SETUP

We have used the 2 $\frac{1}{2}$-dimensional electromagnetic PIC code described in Hesse *et al.*,[23] modified to include the open boundary conditions. For the results presented here, lengths are normalized with respect to the ion inertial length $d_i=c/\omega_i=c(e^2n_0/\varepsilon_0 m_i)^{-1/2}$ using a current sheet density n_0, time is normalized to the inverse ion cyclotron frequency $\Omega_i=eB_0/m_i$ in the asymptotic magnetic field B_0, and velocities are normalized to the Alfvén speed at n_0 and B_0. We use an $(x\text{-}z)$ coordinate system with the x and z directions in the outflow and inflow directions, respectively. The system size is $L_x=L_z=160d_i$ with the system unusually extended in the z direction to provide a large reservoir of particles and magnetic flux for processing through the reconnection site. The initial equilibrium configuration is a Harris sheet

$$B_x=\tan(z/\lambda) \tag{1}$$

with an additional perturbation given by

$$B_{xp}=-\frac{a_0\pi}{L_z}\sin(\pi x/L_x)\sin(\pi z/L_z) \tag{2}$$

and

$$B_{zp}=-\frac{a_0\pi}{L_x}\cos(\pi x/L_x)\cos(\pi z/L_z) \tag{3}$$

with $\lambda=0.5d_i$, $a_0=25.0$, leading to a 10% perturbation field, and with no guide field.

The simulation discussed here was initialized with approximately 2×10^8 particles on an 800×1600 grid in the $x\times z$ directions. Four particle species, two of ions and two of electrons, with mass ratio $m_i/m_e=25$ were included. The "foreground" set of ions and electrons was initialized to establish the pressure and current densities required by Eqs. (1)–(3) and the "background" set was initialized to provide a constant background density $n_b=0.2$. Background and foreground particle temperatures were set equal with $T_i=T_e=0.25$. Using the asymptotic magnetic field to define the electron cyclotron frequency $\Omega_e=eB_0/m_e$ and the plasma sheet density n_0 for the electron plasma frequency $\omega_e=(e^2n_0/\varepsilon_0 m_e)^{1/2}$, we set $\omega_e/\Omega_e=2$.

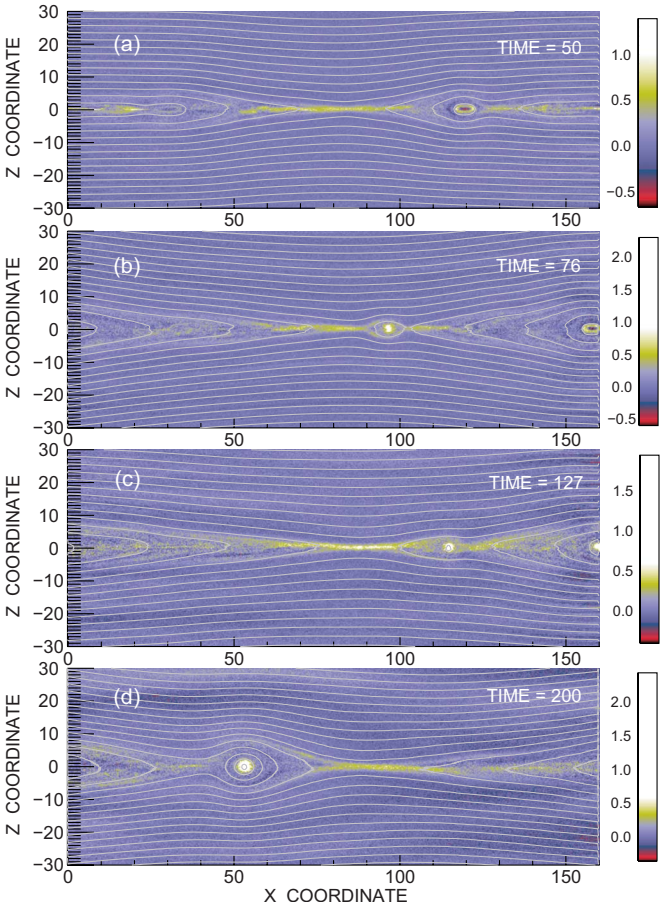

FIG. 2. (Color online) Out-of-plane electron current and magnetic field lines for selected times covering the majority of the simulation. The images have been limited to the portion $z = \pm 30d_i$ of the larger simulation domain. In panels (b)–(d), the upper portions of the color scales have been stretched to place the same blue color at zero current in all panels. Thus, the figure gives a reasonable visual impression of the relative current strengths in the neighborhood of the x line at the times shown in the panels.

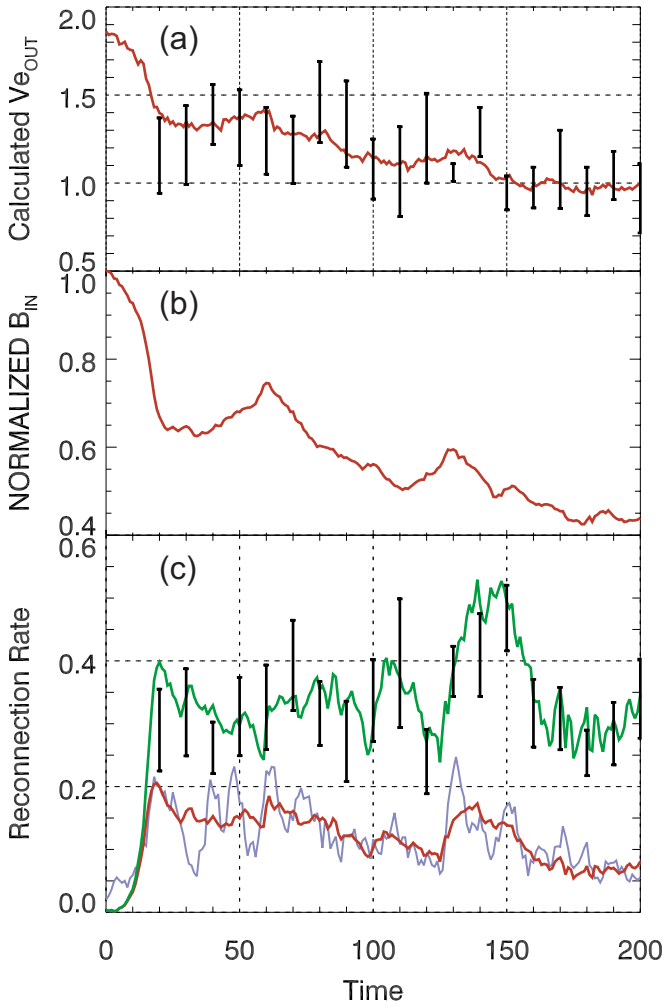

FIG. 3. (Color online) (a) Electron outflow speed at boundary to electron diffusion region as predicted by Eq. (9) (red curve) and measured outflow speed averaged over outflow boundaries of fits to the electron diffusion region (error bars). (b) B_x magnitude near inflow boundary of electron diffusion region normalized by its initial value. (c) Measured reconnection flux transfer rate (red curve), measured out-of-plane electric field in x line neighborhood (blue curve), scaled flux transfer rate (green curve), and basic reconnection rate $r^*(t)$ as given by Eq. (6) (error bars).

IV. SIMULATION RESULTS

For the simulation discussed here, the computational domain was extended in the anti-inflow directions to increase the initial reservoir of particles and magnetic flux for processing through the reconnection site, thereby allowing a study of the long-time evolution of the reconnection process. The magnetic flux content in the simulation domain was monitored as the simulation ran. The position of the dominant x line was followed by finding the minimum in x of the flux

$$\Phi(x,t) = \frac{1}{2}\int_{z\ \min}^{z\ \max} |B_x| dz. \tag{4}$$

The run was stopped at $200\Omega_i^{-1}$ when the total flux at the position of this x line had reduced to approximately 60% of its original value.

Figure 2 gives an overview of the simulation; the electron flux and the magnetic field lines are displayed at selected times. The formation and propagation of several magnetic islands out of the simulation domain, through the open boundaries, is shown. Reconnection begins in this simulation with the formation of several magnetic islands at the tearing wavelength. Panel (a) shows two magnetic islands that are remnants of this initial transient as they propagate toward the outflow boundaries. In panel (b), the island that was on the left in panel (a) has passed out of the simulation domain and the island that was on the right in panel (a) is just at the open boundary on the right. Notice that, in panel (b), an island has formed in the interim and at this time it is propagating toward the open boundary to the right. In panel (c), this island is just passing through the right boundary and another island has formed that is also propagating toward the open boundary to the right. Also in panel (c), a slight brightening in the image can be seen at the position of the x line. Another island is just forming at this time that will later move off toward the left boundary. Panel (d) shows the position of this island at the end of the simulation; it is continuing toward the left boundary.

Using the definition of flux $\Phi(x,t)$ given by Eq. (4), the red curve in the bottom panel of Fig. 3 shows the flux trans-

fer rate, $d\Phi/dt \equiv \dot{\Phi}$, at the evolving position of the dominant x line as given by the minimum in x of $\Phi(x,t)$ at any instant t. The blue curve, in good agreement, shows the out-of-plane component of the electric field at the position of the x line; it has been running-box-car averaged over five output time steps of $1\Omega_i^{-1}$ each. As discussed in the preceding paragraph, magnetic islands that were remnants of the initial transient moved toward and through the outflow boundaries early in the simulation. Subsequently, three magnetic islands formed over the remainder of the simulation; the first at $t \simeq 60$, the second at $t \simeq 100$, and the third at $t \simeq 127$. The first island passed out of the simulation domain through the boundary at the right at $t \simeq 127$, the second at $t \simeq 150$, and the third remained moving toward the left boundary at the end of the simulation As can be seen from Fig. 3, the formation of the first of these islands had no discernible effect on the flux transfer rate or the reconnection electric field, the formation of the second island might have had an effect on these two quantities, and the formation of the third island led directly to a significant temporary increase in these two quantities, reminiscent in this third case of the results of Daughton *et al.*[31] and Karimabadi *et al.*[32]

In the Appendix, we discuss the results of a simulation carried out on an extended domain with periodic outflow boundary conditions. This periodic simulation was set up so that it was expected to reproduce the early evolution of the open boundary simulation, assuming that the open boundary construct works properly. In the periodic simulation, soon after the initial transient stage a magnetic island formed that was associated with a significant temporary increase in the flux transfer rate. During this interval, the flux transfer rate of the periodic simulation was higher than that of the open boundary simulation. Before and after this interval, however, the flux transfer rates of the two simulations were found in good agreement, thus providing increased confidence in the open boundary simulation.

In agreement with the earlier papers discussed above,[31–34] we find a thin out-of-plane electron current sheet and electron outflow jets extended over 10's of ion inertial lengths in the directions of the outflow boundaries of the open boundary simulation. Representative examples from the simulation at $t=50$ are shown in the second and third panels of Fig. 4. At this time, the local ion inertial length is approximately twice the length used to normalize the simulation output and annotate the figures, but the characterization, 10's of ion inertial lengths, remains. Following the early pulse in the flux transfer rate and the reconnection electric field at $t \simeq 20$, we find fluctuations in the overall lengths of the current sheet and outflow jets related primarily to the formation and release of magnetic islands but no trends in their lengths with increasing time, as can be seen from Fig. 2. These appear to be reasonably stable features of the reconnection configuration during this interval.

We have studied the spatial distribution of the electron inertial contribution to the out-of-plane electric field,

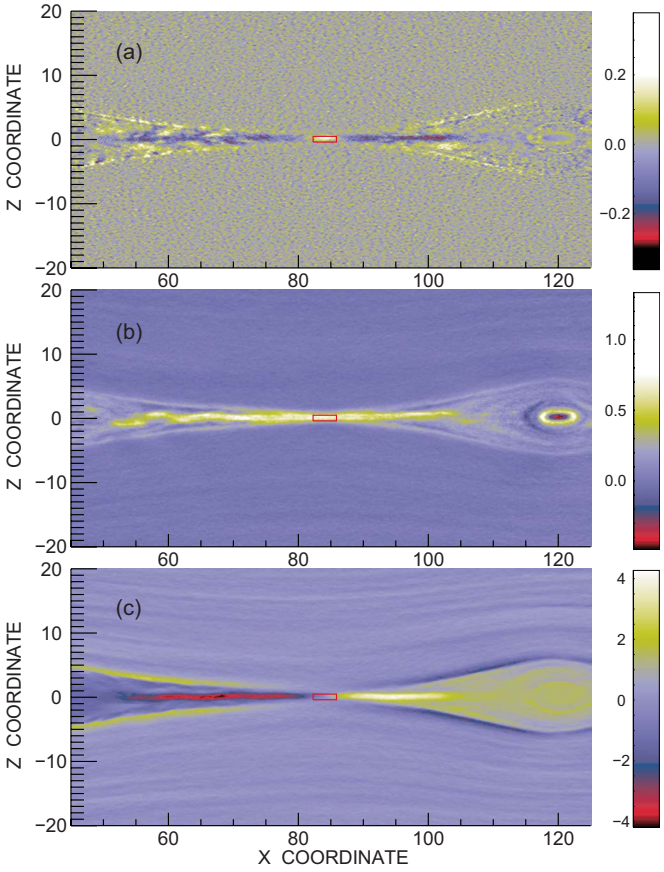

FIG. 4. (Color online) For a small portion of the simulation domain centered on the position of the x line at $t=50\ \Omega_i^{-1}$, (a) the electron inertial contribution to the out-of-plane electric field, (b) the out-of-plane electron current, and (c) the x component of the electron velocity. The red rectangle shows an example of one of the fits to the electron diffusion region; it appears at the same position in all panels. All panels show the results of averaging over an interval $0.2\ \Omega_i^{-1}$. The color scale of panel (a) has been stretched to place gray at zero electric field and compressed to increase the contrast between regions of positive and negative field. The color scale of panel (b) has been stretched as explained in the caption of Fig. 2 for compatibility with that figure.

$$E_y^* = -\left[\frac{1}{en_e}\nabla\cdot\mathbf{P}_e + \frac{m_e}{e}\left(\frac{\partial \mathbf{v}_e}{\partial t} + \mathbf{v}_e\cdot\nabla\mathbf{v}_e\right)\right]_y \tag{5}$$

while, however, ignoring the contribution of the time derivative in Eq. (5). An example of this inertial field is shown in the top panel of Fig. 4 at $t=50$ in the simulation. Notice that the color-scale for this figure has been compressed to increase the contrast of the figure and shifted so that the gray band between yellow and blue lies at $E_y^*=0$; yellow denotes positive field and blue negative. As can be seen from the figure, there are two dominant features in the distribution of this field. There is an inner region of positive field, the electron diffusion region, in which the flux transfer takes place, and two outer regions, coincident with the extended electron outflow jets, where the field is negative indicating that the electrons are outrunning the magnetic field toward the outflow boundaries. These features have been discussed in detail[31–34] but with the terminology, electron diffusion region, applied collectively to both the inner and outer regions where $E_y^* \neq 0$. We will argue below that the label—electron

diffusion region—is more appropriately applied only to the region where $E_y^* > 0$.

Here, we add to this earlier work with a discussion of the aspect ratio of the electron diffusion region over the course of the simulation. For a collection of snapshots such as the one shown in Fig. 4 (but zoomed in much further), a rectangle has been fit visually to the electron diffusion region; the red box shown in all panels of Fig. 4 is an example of such a fit. We find that the total width d of the rectangle in the z direction remains close to $\frac{1}{2}$ local ion inertial length and the total length L in the z direction varies in the range 2–3 local ion inertial lengths. The aspect ratio d/L was determined for each of these snapshots.

Using $v_{e_{\text{in}}} n_{e_{\text{in}}} L = v_{e_{\text{out}}} n_{e_{\text{out}}} d$ in terms of the electron inflow and outflow speeds and densities at the boundaries of the rectangle, we can write a reconnection rate

$$r(t) \equiv \frac{v_{e_{\text{in}}}}{v_{eA_{\text{in}}}} = \frac{v_{e_{\text{out}}}}{\sqrt{2} v_{eA_{\text{in}}}} \left[\sqrt{2} \frac{n_{e_{\text{out}}}}{n_{e_{\text{in}}}} \left(\frac{d}{L} \right) \right] \equiv \frac{v_{e_{\text{out}}}}{\sqrt{2} v_{eA_{\text{in}}}} r^*(t) \quad (6)$$

in terms of the aspect ratio d/L. In Eq. (6), $v_{e_{\text{in}}}$ is the electron inflow speed at the inflow boundary, $v_{eA_{\text{in}}}$ is the electron Alfvén speed at the inflow boundary, $v_{e_{\text{out}}}$ is the electron outflow speed at the outflow boundary, and $n_{e_{\text{in}}}$ and $n_{e_{\text{out}}}$ are the electron densities at the inflow and outflow boundaries, respectively. If we assume that all of the inflowing magnetic energy is converted to outgoing electron kinetic energy, then it is easy to show that $v_{e_{\text{out}}} = \sqrt{2} v_{eA_{\text{in}}}$ and, at this basic level of approximation, the reconnection rate $r(t) = r^*(t)$. Below, we show that this is a poor estimate for $v_{e_{\text{out}}}$ but, even so, this basic reconnection rate estimate $r^*(t)$ will play an important role in our discussion. To evaluate $r^*(t)$, we have measured the densities (and other quantities discussed below) at the inflow and outflow boundaries by placing another rectangle centered at $z=0$ and at the x position of the x line, as given by the magnetic flux minimum discussed above, with dimensions $\pm 2 d_i$ in the x and z directions; the densities (and other quantities) were measured at the perimeter of this rectangle. By comparing this rectangle to the manual fits to the electron diffusion region, we have found that the length of this rectangle is equal to a typical length of the variable diffusion region and that the width is in the range 2–3 times the total width of the diffusion region. Thus, with this fixed dimension rectangle suitable for automatic numerical application, outflow quantities are measured at the typical position of the outflow boundaries and inflow quantities are measured just outside of the actual diffusion region. The error bars in the bottom panel of Fig.3 show the evolution of the basic reconnection rate $r^*(t)$, so determined. Because there is considerable background noise in our images of E_y^*, as can be seen from the top panel of Fig. 4, and because our fitting procedure is subjective, we have constructed a set of what we judge to be the most extreme interpretations of d/L consistent with the images; the upper and lower ends of the error bars show these extremes.

In contrast to the open boundary simulations due to Daughton *et al.*[31] and Karimabadi *et al.*,[32] plasma is not replenished at the boundaries of the inflow regions of our simulation domain. We have emulated the flux transfer rate that we might have obtained in a fully open boundary simulation by scaling the flux transfer rate $\dot{\Phi}(t)$,

$$\dot{\Phi}_S(t) = \left(\frac{B_{x_{\text{in}}}(t=0)}{B_{x_{\text{in}}}(t)} \right)^2 \sqrt{\frac{n_{e_{\text{in}}}(t)}{n_{e_{\text{in}}}(t=0)}} \dot{\Phi}(t) \quad (7)$$

to take into account changes in field strength and electron density at the inflow boundaries of the electron diffusion region as the simulation advances. These quantities were measured at the inflow boundaries of the fixed dimension rectangle discussed in the preceding paragraph. The density ratio in Eq. (7), although included, never gets far from 1 and its effect is minimal. The evolution of the magnetic field ratio in Eq. (7) is shown in panel (b) of Fig. 3 and the evolution of the scaled flux transfer rate is shown by the green curve in the bottom panel.

Initially, the real and scaled flux transfer rates are in agreement. Due to the typical large burst of reconnection early in the simulation, however, the magnetic field strength at the inflow boundary of the electron diffusion regions drops precipitously, leading to a large and slightly delayed peak in the scaled flux transfer rate. The field strength then takes on a slow and, on average, steady decline as the remaining magnetic flux available for reconnection lowers. This decline is at just the required rate to lead to a fluctuating but, on average, steady scaled flux transfer rate until the last magnetic island forms near the end of the simulation. The scaled transfer rate is high, in the range 0.2–0.4 during most of this interval due, primarily, to the large drop in magnetic field strength at the inflow boundary early in the simulation. The second reconnection burst associated with the formation and release of the third magnetic island at $t \simeq 127$ leads to a large peak in the scaled flux transfer rate that is amplified by the continuously decreasing inflow field strength.

From the bottom panel of Fig. 3, we can see that the scaled flux transfer rate $\dot{\Phi}_S(t)$ and the basic reconnection rate $r^*(t)$ are largely in agreement. Interestingly, we find that $r^*(t)$ tracks the large peak in the scaled flux transfer rate quite nicely. Thus we conclude that $r^*(t)$, computed on the basis of the aspect ratio of the electron diffusion region, predicts the scaled flux transfer rate and we hypothesize that in a steady reconnection simulation $r^*(t)$ would yield the true flux transfer rate. On this basis, we suggest that it is the electron diffusion region, as we have defined it, that is controlling the reconnection flux transfer rate.

Equating $r^*(t)$ with $\dot{\Phi}_S(t)$, as suggested by Fig. 3, yields a relation from which we can compute the electron outflow speed $v_{e_{\text{out}}}$ at the outflow boundary of the electron diffusion region. Assuming that $r^*(t) = \dot{\Phi}_S(t)$, from Eqs. (6) and (7) we find

$$r(t) = \frac{v_{e_{\text{in}}} B_{x_{\text{in}}}}{v_{eA_{\text{in}}} B_{x_{\text{in}}}} = \frac{\dot{\Phi}}{v_{eA_{\text{in}}} B_{x_{\text{in}}}} = \frac{v_{e_{\text{out}}}}{\sqrt{2} v_{eA_{\text{in}}}} r^*(t)$$
$$= \frac{v_{e_{\text{out}}}}{\sqrt{2} v_{eA_{\text{in}}}} \left(\frac{B_{x_{\text{in}}}(t=0)}{B_{x_{\text{in}}}(t)} \right)^2 \sqrt{\frac{n_{e_{\text{in}}}(t)}{n_{e_{\text{in}}}(t=0)}} \dot{\Phi} \tag{8}$$

in which we have used $v_{e_{\text{in}}} B_{x_{\text{in}}} = \dot{\Phi}$. Equating the two terms in this expression containing the common $\dot{\Phi}$, we find

$$v_{e_{\text{out}}} = \frac{\sqrt{2}}{B_{x_{\text{in}}}(t=0)} \sqrt{\frac{n_{e_{\text{in}}}(t=0)}{n_{e_{\text{in}}}(t)}} \left(\frac{B_{x_{\text{in}}}(t)}{B_{x_{\text{in}}}(t=0)} \right). \tag{9}$$

The red curve in the top panel of Fig. 3 shows the electron outflow speed computed from Eq. (9) using the fixed dimension rectangle on which to measure these incoming quantities. While this outflow speed may seem unusually small, it should be noted that most of the outflow acceleration takes place downstream of the boundaries of the electron diffusion region, as can be seen in the bottom panel of Fig. 4. At the boundaries, much of the incoming field energy still resides in the out-of-plane motion of the electrons. To confirm Eq. (9), the electron outflow speed has been averaged over the outflow boundaries of the fits to the electron diffusion region used to compute the aspect ratio of the region (such as the one shown by the red rectangle in the panels of Fig. 4). The resulting averages are illustrated by the error bars in the top panel of Fig. 3. Again, the error bars indicate the uncertainty in the results due to the uncertainty in the fits. We interpret this result as confirmation of Eq. (9) and, more importantly, of the more fundamental equality $r^*(t) = \dot{\Phi}_S(t)$, which was used to obtain Eq. (9).

V. DISCUSSION AND CONCLUSIONS

We have introduced a new method for imposing open boundary conditions on PIC simulations and have discussed the results of a 2 $\frac{1}{2}$-dimensional PIC reconnection simulation using these open conditions at the outflow boundaries and simple reflecting boundaries to the inflow regions. We have extended the computational domain in the directions of the reflecting boundaries to increase the initial reservoir of particles and magnetic flux for processing through the reconnection site, thereby allowing a study of the long-time evolution of the reconnection process. We have followed the flux transfer rate at the position of the dominant x line and have computed a scaled flux transfer rate to account for the decline with increasing time of the magnetic field strength and electron density at the inflow boundary to the electron diffusion region. We have obtained a fast scaled flux transfer rate with fluctuations but with no decreasing trend with increasing time. We have obtained some magnetic island formation after the initial transients in the simulation. The first of these produced no discernible effect on the reconnection rate, while the second is coincident with a weak peak that may be due to an unrelated fluctuation. The third produced a temporary but dramatic increase in the reconnection rate, in agreement with the findings of Daughton *et al.*[31] and Karimabadi *et al.*[32] We have also carried out a periodic boundary simulation on an extended domain to successfully verify the validity of the open boundary simulation. Interestingly, early in the periodic simulation, a magnetic island formed that produced a significant temporary increase in the reconnection rate, in contrast to the early behavior of the open boundary simulation. At this time, we do not understand why some islands have no effect on the reconnection rate but others do. In agreement with earlier studies, we note the formation of a thin out-of-plane electron current sheet extended in the outflow directions for tens of ion inertial lengths. The length of this current sheet fluctuates over the course of the simulation but does not exhibit an increasing trend with time. In further agreement with earlier work, we find intense, thin, electron outflow jets that reach far from the x line. We have examined the evolution of the electron diffusion region. This region varies in the range 2.5–4 local electron inertial lengths in total width and in the range 10–15 local electron inertial lengths in total length over the course of the simulation. We have measured the aspect ratio of this region and have used it to compute a basic reconnection rate using inflow and outflow conditions at the diffusion region boundaries. We have found that this basic reconnection rate is in agreement with the scaled flux transfer rate over the course of the simulation. We hypothesize that in a steady reconnection simulation, this basic reconnection rate, with its dependence on the aspect ratio of the electron diffusion region, will yield the true flux transfer rate. Further, we conclude that the electron diffusion region proper either adjusts its geometry for compatibility with the reconnection rate that is set elsewhere, as in the Hall reconnection model, or that it is this region that actually controls the reconnection flux transfer rate.

ACKNOWLEDGMENTS

This research was supported by NASA's MMS mission. One of us (S.Z.) gratefully acknowledges support from NASA's postdoctoral program.

APPENDIX: PERIODIC OUTFLOW BOUNDARY SIMULATION

Since the open boundary construct introduced in this paper is new, it is important to validate the simulation results that have been discussed in Sec. IV. To that end, we have carried out an analogous simulation using periodic outflow boundary conditions on a simulation domain extended in the outflow directions to reduce the effects of the boundary conditions in the x-line neighborhood early in the simulation.

From Eqs. (2) and (3), it can be seen that the initial perturbation used in the open boundary simulation extended over $\frac{1}{2}$ period of the trig-functions that appear in those equations. To set up the periodic simulation, the length of the simulation domain was doubled to $L_x = 320 d_i$ while holding the x dependence of the initial perturbation fixed. The initial perturbation then extended over an entire period of the trig-functions and was compatible with the assumption of periodic outflow boundary conditions, i.e.,

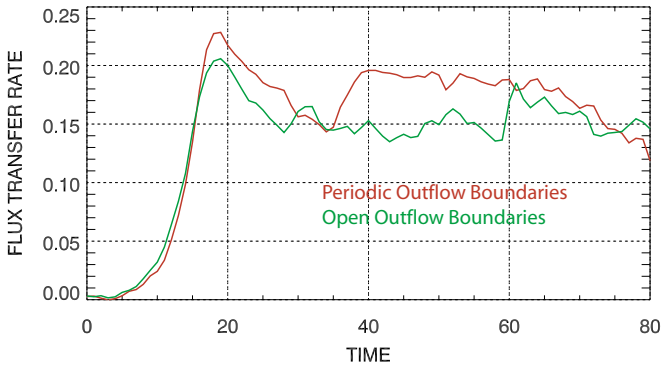

FIG. 5. (Color online) Flux transfer rate $\dot{\Phi}$ for (red) periodic boundary simulation and (green) open boundary simulation as a function of time in inverse ion cyclotron periods.

$$B_{xp} = \frac{a_0 \pi}{L_z} \cos(2\pi x/L_x)\sin(\pi z/L_z) \tag{A1}$$

and

$$B_{zp} = -\frac{a_0 2\pi}{L_x} \sin(2\pi x/L_x)\cos(\pi z/L_z) \tag{A2}$$

with the doubled $L_x = 320 d_i$. To maintain the same grid spacing and initial particle density in both simulations, the number of grid points in the periodic simulation was doubled to 1600 in the x direction and the initial number of particles was doubled to approximately 4×10^8. All other quantities given in Sec. III for the open boundary simulation setup were unchanged. Unfortunately, as the outflow jets were established in the open boundary simulation, the number of particles in that simulation decreased with time and consequently the particle densities in the two simulations diverged.

From the definition of flux $\Phi(x,t)$ given by Eq. (4), the flux transfer rate has been defined as $d\Phi/dt \equiv \dot{\Phi}$ at the evolving position of the dominant x line as given by the minimum in x of $\Phi(x,t)$ at any instant t. Figure 5 shows a comparison of the flux transfer rates obtained from the periodic and open boundary simulations. Over the interval shown in the figure, no disturbances from the collisions of the outflow jets at the boundaries of the periodic simulation were detected in the central region of that simulation of an extent equal to that of the entire open boundary simulation domain.

Initially, the two flux transfer rates tracked each other quite well, peaking simultaneously with the periodic boundary rate exceeding the open boundary rate somewhat. Interestingly, shortly after the two rates joined at $\sim 30\ \Omega_i^{-1}$, the periodic rate increased suddenly due to the formation of a magnetic island (not shown) in accordance with the findings of Daughton *et al.*[31] and Karimabadi *et al.*[32] This behavior is in contrast to that of the open boundary simulation in which the early formation of magnetic islands did not lead to discernible fluctuations in the flux transfer rate. The factors that do or do not lead to this response in the flux transfer rate remain unknown at this time.

In Fig. 5, as the magnetic island induced burst in the flux transfer rate in the periodic simulation subsides, the transfer rates of the two simulations join approximately for the remainder of the interval shown. Up to the formation of the magnetic island in the periodic simulation, comparisons (not shown) of the outflow jet and current sheet geometries in the two simulations have revealed remarkably similar results. We take these comparisons plus that shown in Fig. 5 as substantial evidence for the success of the open boundary construct.

[1] E. N. Parker, J. Geophys. Res. **62**, 509, DOI: 10.1029/JZ062i004p00509 (1957).
[2] E. N. Parker, Astrophys. J. **330**, 474 (1988).
[3] M. J. Aschwanden, *Physics of the Solar Corona: An Introduction* (Springer, Berlin, 2004).
[4] J. Lin, Y. K. Ko, L. Sui, J. C. Raymond, G. A. Stenborg, Y. Jiang, S. Zhao, and S. Mancuso, Astrophys. J. **622**, 1251 (2005).
[5] J. Jing, J. Qiu, J. Lin, M. Qu, Y. Xu, and H. M. Wang, Astrophys. J. **620**, 1085 (2005).
[6] J. T. Gosling, S. Eriksson, D. J. McComas, T. D. Phan, and R. M. Skoug, J. Geophys. Res. **112**, 10111, DOI: 10.1029/2007JA012418 (2007).
[7] J. T. Gosling, S. Eriksson, and R. Schwenn, J. Geophys. Res. **111**, 10102, DOI: 10.1029/2006JA011863 (2006).
[8] T. D. Phan, J. T. Gosling, M. S. Davis, R. M. Skoug, M. Oieroset, R. P. Lin, R. P. Lepping, D. J. McComas, C. W. Smith, H. Reme, and A. Balogh, Nature (London) **439**, 175 (2006).
[9] J. W. Dungey, Phys. Rev. Lett. **6**, 47 (1961).
[10] A. Retino, D. Sundkvist, A. Vaivads, F. Mozer, M. Andre, and C. J. Owen, Nat. Phys. **3**, 235 (2007).
[11] F. S. Mozer, S. D. Bale, and T. D. Phan, Phys. Rev. Lett. **89**, 015002 (2002).
[12] F. S. Mozer, S. D. Bale, T. D. Phan, and J. A. Osborne, Phys. Rev. Lett. **91**, 245002 (2003).
[13] C. T. Russell, K. K. Khurana, D. E. Huddleston, and M. G. Kivelson, Science **280**, 1061 (1998).
[14] V. Sergeev, V. Semenov, M. Kubyshkina, V. Ivanova, W. Baumjohann, R. Nakamura, T. Penz, A. Runov, T. L. Zhang, K. H. Glassmeier, V. Angelopoulos, H. Frey, J. A. Sauvaud, P. Daly, J. B. Cao, H. Singer, and E. Lucek, Geophys. Res. Lett. **34**, 02103, DOI: 10.1029/2006GL028452 (2007).
[15] T. Nagai, M. Fujimoto, Y. Saito, S. Machida, T. Terasawa, R. Nakamura, T. Yamamoto, T. Mukai, A. Nishida, and S. Kokubun, J. Geophys. Res. **103**, 4419, DOI: 10.1029/97JA02190 (1998).
[16] M. Oieroset, T. D. Phan, M. Fujimoto, R. P. Lin, and R. P. Lepping, Nature (London) **412**, 414 (2001).
[17] H. T. Ji, S. Terry, M. Yamada, R. Kulsrud, A. Kuritsyn, and Y. Ren, Phys. Rev. Lett. **92**, 115002 (2004).
[18] Y. Ren, M. Yamada, S. Gerhardt, H. T. Ji, R. Kulsrud, and A. Kuritsyn, Phys. Rev. Lett. **95**, 055003 (2005).
[19] R. Kulsrud, H. T. Ji, W. Fox, and M. Yamada, Phys. Plasmas **12**, 8 (2005).
[20] F. V. Coroniti, Astrophys. J. **349**, 538 (1990).
[21] P. P. Kronberg, S. A. Colgate, H. Li, and Q. W. Dufton, Astrophys. J. Lett. **604**, L77 (2004).
[22] M. Hesse and D. Winske, J. Geophys. Res. **99**, 11177, DOI: 10.1029/94JA00676 (1994).
[23] M. Hesse, K. Schindler, J. Birn, and M. Kuznetsova, Phys. Plasmas **6**, 1781 (1999).
[24] M. Hesse, J. Birn, and M. Kuznetsova, J. Geophys. Res. **106**, 3721, DOI: 10.1029/1999JA001002 (2001).
[25] M. E. Mandt, R. E. Denton, and J. F. Drake, Geophys. Res. Lett. **21**, 73, DOI: 10.1029/93GL03382 (1994).
[26] M. A. Shay, J. F. Drake, M. Swisdak, and B. N. Rogers, Phys. Plasmas **11**, 2199 (2004).
[27] B. N. Rogers, R. E. Denton, J. F. Drake, and M. A. Shay, Phys. Rev. Lett. **87**, 195004 (2001).
[28] D. Biskamp and E. Schwarz, Phys. Plasmas **8**, 4729 (2001).
[29] J. Birn, J. F. Drake, M. A. Shay, B. N. Rogers, R. E. Denton, M. Hesse,

M. Kuznetsova, Z. W. Ma, A. Bhattacharjee, A. Otto, and P. L. Pritchett, J. Geophys. Res. **106**, 3715, DOI: 10.1029/1999JA900449 (2001).
[30]M. A. Shay, J. F. Drake, B. N. Rogers, and R. E. Denton, Geophys. Res. Lett. **26**, 2163, DOI: 10.1029/1999GL900481 (1999).
[31]W. Daughton, J. Scudder, and H. Karimabadi, Phys. Plasmas **13**, 072101 (2006).
[32]H. Karimabadi, W. Daughton, and J. Scudder, Geophys. Res. Lett. **34**, 13104, DOI: 10.1029/2007GL030306 (2007).
[33]K. Fujimoto, Phys. Plasmas **13**, 072904 (2006).
[34]M. A. Shay, J. F. Drake, and M. Swisdak, Phys. Rev. Lett. **99**, 155002 (2007).
[35]A. B. Langdon, Comput. Phys. Commun. **70**, 447 (1992).